Dynamical Formation of Low-mass Merging Black Hole Binaries like GW151226

Citation: Chatterjee, Sourav; Rodriguez, Carl L.; Kalogera, Vicky and Rasio, Frederic A. "Dynamical Formation of Low-Mass Merging Black Hole Binaries Like GW151226." The Astrophysical Journal Letters 836, no. 2 (February 2017): L26. © 2017 The American Astronomical Society

As Published: http://dx.doi.org/10.3847/2041-8213/aa5caa

Publisher: IOP Publishing

Persistent URL: http://hdl.handle.net/1721.1/109698

Version: Final published version: final published article, as it appeared in a journal, conference proceedings, or other formally published context

The Astrophysical Journal Letters, 836:L26 (7pp), 2017 February 20 https://doi.org/10.3847/2041-8213/aa5caa

Dynamical Formation of Low-mass Merging Black Hole Binaries like GW151226

Sourav Chatterjee[1], Carl L. Rodriguez[1,2], Vicky Kalogera[1], and Frederic A. Rasio[1]
[1] Center for Interdisciplinary Exploration & Research in Astrophysics (CIERA) Physics & Astronomy, Northwestern University, Evanston, IL 60202, USA; sourav.chatterjee@northwestern.edu
[2] MIT-Kavli Institute for Astrophysics and Space Research, 77 Massachusetts Avenue, 37-664H, Cambridge, MA 02139, USA
Received 2016 September 21; accepted 2017 January 28; published 2017 February 17

Abstract

Using numerical models for star clusters spanning a wide range in ages and metallicities (Z) we study the masses of binary black holes (BBHs) produced dynamically and merging in the local universe ($z \lesssim 0.2$). After taking into account cosmological constraints on star formation rate and metallicity evolution, which realistically relate merger delay times obtained from models with merger redshifts, we show here for the first time that while old, metal-poor globular clusters can naturally produce merging BBHs with heavier components, as observed in GW150914, lower-mass BBHs like GW151226 are easily formed dynamically in younger, higher-metallicity clusters. More specifically, we show that the mass of GW151226 is well within 1σ of the mass distribution obtained from our models for clusters with $Z/Z_{\odot} \gtrsim 0.5$. Indeed, dynamical formation of a system like GW151226 likely requires a cluster that is younger and has a higher metallicity than typical Galactic globular clusters. The LVT151012 system, if real, could have been created in any cluster with $Z/Z_{\odot} \lesssim 0.25$. On the other hand, GW150914 is more massive (beyond 1σ) than typical BBHs from even the lowest-metallicity ($Z/Z_{\odot} = 0.005$) clusters we consider, but is within 2σ of the intrinsic mass distribution from our cluster models with $Z/Z_{\odot} \lesssim 0.05$; of course, detection biases also push the observed distributions toward higher masses.

Key words: black hole physics – galaxies: star clusters: general – globular clusters: general – gravitational waves – methods: numerical – methods: statistical

1. Introduction

Detection of gravitational waves (GWs) from merging black hole (BH) binaries has reignited widespread interest in understanding the astrophysical implications and the origins of binary black holes (BBHs; Abbott et al. 2016a, 2016c, 2016d). Current theoretical estimates indicate that detectable BBH merger events may be rather frequent, few—$500\,\mathrm{Gpc^{-3}\,yr^{-1}}$, with large uncertainties depending on production channels and model assumptions (e.g., compare Rodriguez et al. 2016a; Askar et al. 2017 with de Mink & Mandel 2016). In the first observing run itself, the advanced LIGO observatories (aLIGO) have detected GW signals from two BBH mergers and a lower significance "trigger" event (Abbott et al. 2016b, 2016c, 2016d). These detections already show a large diversity in the masses of BBHs merging in the local universe: the chirp masses ($M_{\rm chirp}$) at source for GW150914, LVT151012, and GW151226 are 28^{+2}_{-2}, 15^{+1}_{-1}, and $8.9^{+0.3}_{-0.3}$, respectively.

Broadly speaking, two major channels have been proposed for BBH formation and subsequent merger. High-mass stellar binaries may evolve in isolation to create merging BBHs, for example, by going through a specific sequence of events involving low-kick supernovae (SNe) and common-envelope (CE) evolution (e.g., Dominik et al. 2012, 2013, 2015; Belczynski et al. 2014, 2016a, 2016b; Kowalska-Leszczynska et al. 2015), and via chemically homogeneous evolution of tidally distorted binaries (e.g., Mandel & de Mink 2016; Marchant et al. 2016).

Alternatively, merging BBHs could be produced dynamically at the centers of dense star clusters (e.g., Banerjee et al. 2010; Ziosi et al. 2014; Rodriguez et al. 2015, 2016a). The process involved here is fundamentally different from BBH formation in isolation. A negligible fraction of BBHs formed in dense massive star clusters are primordial, and none with $t_{\rm delay} \geqslant 1\,\mathrm{Gyr}$ are composed of BHs formed from stars that were born in that binary (e.g., Chatterjee et al. 2017). As massive stellar binaries evolve in dense star clusters, even if they were initially hard, mass loss from stellar winds and compact object formation can make these binaries soft. Consequently, stellar encounters and natal kicks during BH formation disrupt these primordial binaries. Later, single BHs dynamically acquire other BH companions via three-body binary formation and binary-mediated exchange interactions that preferentially insert the relatively more massive BHs into a binary ejecting a less massive non-BH member from it (e.g., Heggie & Hut 2003; Chatterjee & Tan 2012). Because of this, the BBH properties and their merger times, unlike those formed in isolation, do not depend on the assumptions of initial binarity or binary orbital properties. While the rate of mergers is affected by the assumptions for the IMF and natal kicks, the BBH masses and merger delay times ($t_{\rm delay}$) are insensitive to those as well (Chatterjee et al. 2017).

While several studies have modeled BBH formation in isolation for a wide range in metallicities taking into account the cosmological evolutions of the star formation rate (SFR) and metallicity (e.g., Belczynski et al. 2016a; de Mink & Mandel 2016; Dvorkin et al. 2016), due to primarily the computational cost, numerical studies of dynamically formed BBHs have so far restricted themselves to either a narrow range in metallicities and ages typical of the Galactic globular clusters (GGCs; e.g., Rodriguez et al. 2015; Chatterjee et al. 2017) or to low-mass (initial $N \sim 5 \times 10^3$), young ($\sim$100 Myr) star clusters (e.g., Ziosi et al. 2014). These studies also assumed that all model clusters formed roughly at the same epoch independent of the metallicity to evaluate the redshifts of BBH mergers from $t_{\rm delay}$ found in the models. This of course is a simplification. Stars form with wide ranges in metallicities at any redshift (e.g., Madau & Dickinson 2014). Massive star

clusters are also observed today with a large range in ages and metallicities, for example, in M51, M101, and the LMC (e.g., Bastian et al. 2005; Barmby et al. 2006; Scheepmaker et al. 2007). Even for the GGCs, the metallicity distribution has a long tail extending to $Z_\odot$ (Harris 1996).

We relax past assumptions and consider BBH formation and merger in clusters spanning a wide range in metallicities and metallicity-dependent distributions for cluster formation redshifts ($z_{\rm form}$). Our goal is to investigate whether all hitherto detected GW sources could have been formed dynamically in star clusters. Furthermore, we study effects of star cluster metallicity and age on the detectable properties (mass and eccentricity) of BBH mergers. In Section 2, we describe our numerical setup. In Section 3, we show the key results. We conclude in Section 4.

2. Numerical Models

We use our Hénon-type Monte Carlo cluster dynamics code CMC to model star clusters. CMC includes all physical processes relevant to study BBH production, dynamical evolution, and mergers in star clusters (e.g., Fregeau & Rasio 2007; Chatterjee et al. 2010; Pattabiraman et al. 2013; Rodriguez et al. 2016c). The initial structural properties are guided by those of the observed young massive clusters, thought to be similar in properties (except metallicity) to the progenitors of today's GCs (e.g., Chatterjee et al. 2010, 2013). We use seven different metallicities spanning a large range: $Z/Z_\odot = 0.005$, 0.025, 0.05, 0.25, 0.5, 0.75, and 1. Since we focus on studying the effects of star cluster metallicity on BBH mergers, we fix all other initial properties of our model clusters in the main set: all models initially have $N = 8 \times 10^5$ single/binary stars. The initial positions and velocities are assigned following a King profile with $w_0 = 5$. The initial virial radius $r_v = 2$ pc. The initial stellar masses (primary mass, M_p, in case of a binary) are drawn from the IMF given in Kroupa (2001) between 0.08 and 150 $M_\odot$. The initial binary fraction is $f_b = 10\%$. The secondary masses (M_s) are drawn from a uniform distribution between $0.08/M_p$ and 1. The initial orbital periods for binaries are flat in logarithmic intervals, and the eccentricities (e) are thermal. The single and binary stellar evolution are modeled using the SSE and BSE software (Hurley et al. 2000, 2002) updated with state-of-the-art prescriptions for stellar winds (e.g., Vink et al. 2001) and fallback-dependent natal kick distribution for BHs (e.g., Belczynski et al. 2002; Fryer et al. 2012). To improve statistics, we repeat each model using different seeds.

We create two additional sets of models with $Z/Z_\odot = 0.05$ by varying the initial N and r_v to study their effects. In one set, we change the initial r_v to 1 pc. In the other, we vary the initial N to 2×10^5 and 2×10^6. Relevant model properties are summarized in Table 1.

3. Results

Merging BBHs decrease in mass with increasing metallicity, a direct consequence of the metallicity dependence of the BH mass spectrum at formation (Figure 1; Belczynski et al. 2010). Merging BBHs also decrease in mass as the merger delay time ($t_{\rm delay}$), defined by the time of BBH merger from $t = 0$ for the cluster, increases. This is because clusters form and dynamically process higher-mass BBHs first, followed by less massive ones due to mass segregation (Breen & Heggie 2013; Morscher et al. 2015). Moreover, higher-mass BBHs merge faster due to GW radiation (Peters 1964).

Of all BBH mergers within a Hubble time, the fraction of in-cluster mergers varies between ∼0.3% and 5%. The majority of all BBHs merge long after they are ejected from the cluster predominantly via dynamical scattering in the cluster's core. At most, ∼16% of all mergers involve merging of BHs whose progenitors were initially members of the same binary. Even for these, either the BHs or their progenitors have had at least one strong encounter (typically many), such as binary-mediated scattering, and physical collisions before they merge (similar conclusions in, e.g., Rodriguez et al. 2016b).

3.1. Merger Time Delay versus Redshift

Connecting $t_{\rm delay}$ to merger redshift requires knowledge of the redshift of formation for the parent cluster. We closely follow the approach of Belczynski et al. (2016a) and adopt state-of-the-art cosmological constraints for SFR(z) and Z(z) to infer the $z_{\rm form}$-distribution for clusters with a given metallicity. We adopt

$$\mathrm{SFR}(z) = 0.015\frac{(1+z)^{2.7}}{1+\{(a+z)/2.9\}^{5.6}}\,M_\odot\ \mathrm{Mpc}^{-3}\ \mathrm{yr}^{-1} \quad (1)$$

(Madau & Dickinson 2014). SFR(z) peaks at $z \simeq 2$ (look-back time $t_{\rm lb} \simeq 10$ Gyr), and decreases by a factor of 5 from its peak value by $z = 0.24$ ($t_{\rm lb} \simeq 3$ Gyr) and $z = 5.4$ ($t_{\rm lb} \simeq 12$ Gyr). The mean metallicity, $\overline{\rm Z}$, is given by

$$\log\overline{\rm Z}(z) = K + \log\left(\frac{y(1-R)}{\rho_b}\int_z^{20}\frac{97.8\times10^{10}\mathrm{SFR}(z')}{H_0E(z')(1+z')}dz'\right) \quad (2)$$

(Belczynski et al. 2016a, their Equation (2)). $R = 0.27$ is the mass fraction of a generation of stars that remixes into the interstellar medium, $y = 0.019$ is the net metal production, $\rho_b = 2.77 \times 10^{11}\Omega_b h_0^2\ M_\odot\ \mathrm{Mpc}^{-3}$ is the baryon density, and $E(z) = \sqrt{\Omega_M(1+z)^3 + \Omega_k(1+z)^2 + \Omega_\Lambda}$.[3] We adopt normalization constant $K = 1.30749$ to obtain $\overline{\rm Z} = 0.001$ and 0.02 for $t_{\rm lb} \simeq 12$ and 5 Gyr, respectively, guided by the typical ages and metallicities of the GGCs and the Sun. The exact adopted value of K (within constraints) does not affect our results significantly.

The probability distribution function (PDF) for $z_{\rm form}$ of a given metallicity Z′ is,

$$f(z)_{\rm Z'} = \int_{\rm Z=0.9Z'}^{1.1\rm Z'}\int_{z'=0}^{20}\mathrm{SFR}(z')f'(\mathrm{Z})_{z'}dz'd\mathrm{Z}, \quad (3)$$

where $f'(\mathrm{Z})_z$ is assumed to be lognormal with $\sigma = 0.5$ dex and mean $= \overline{\rm Z}(z)$, given by Equation (2) (Belczynski et al. 2016a). We evaluate $f(z)_{\rm Z'}$ in the following way. We randomly generate 10^5 redshift values between 0 and 20 weighted by SFR(z) (Equation (1)). For each draw of redshift we calculate $\overline{\rm Z}$ and randomly generate 10^2 metallicity values from $f'(\mathrm{Z})_z$. Thus, we generate a database of 10^7 redshift–metallicity pairs. We then collect all redshift values corresponding to metallicities within $\mathrm{Z}' \pm 0.1\mathrm{Z}'$. $f(z)_{\rm Z'}$ is then obtained from these

[3] We assume standard cosmological values: $\Omega_b = 0.045$, $h_0 = 0.7$, $\Omega_\Lambda = 0.7$, $\Omega_M = 0.3$, $\Omega_k = 0$, and $H_0 = 70\ \mathrm{km\ s^{-1}\ Mpc^{-1}}$.

Table 1
Star Cluster Models and BBH Merger Properties

N (10^5)	M_i ($10^5\,M_\odot$)	r_v (pc)	Z/Z$_\odot$	#	Cluster Formation Time		BBH Merger Properties						$N_{\rm merge}$	
					$z_{\rm form}$	$t_{\rm lb}$ (Gyr)	$M_{\rm tot}$ ($M_\odot$)	$M_{\rm chirp}$	$M_{\rm tot}$ ($M_\odot$)	$M_{\rm chirp}$	$\log e_1$	$\log e_{-4}$		
							$z \leqslant 0.2$		$z \leqslant 1$		$z \leqslant 1$		$z \leqslant 0.2$	$z \leqslant 1$
	…	…	0.005	4	$6.2^{+1.9}_{-1.7}$	$12.6^{+0.3}_{-0.4}$	$37.7^{+8.4}_{-7.0}$	$16.4^{+3.5}_{-3.1}$	$39.8^{+9.4}_{-7.4}$	$17.3^{+3.9}_{-3.3}$	$-7.3^{+0.8}_{-0.8}$	$-2.0^{0.8}_{-0.8}$	4^{+4}_{-1}	26^{+2}_{-5}
	…	…	0.025	4	$4.2^{+1.1}_{-1.4}$	$12.0^{+0.4}_{-0.9}$	$37.2^{+7.6}_{-6.8}$	$16.1^{+3.3}_{-2.9}$	$39.2^{+9.9}_{-6.5}$	$16.9^{+4.2}_{-2.8}$	$-7.3^{+1}_{-0.6}$	$-2.0^{+1}_{-0.5}$	4^{+5}_{-1}	24^{+7}_{-1}
	…	…	0.05	4	$3.4^{+1.1}_{-1.1}$	$11.6^{+0.5}_{-1.0}$	$37.6^{+5.9}_{-5.9}$	$16.4^{+2.5}_{-2.7}$	$39.6^{+7.7}_{-6.9}$	$17.1^{+3.4}_{-3.0}$	$-7.2^{+0.8}_{-0.7}$	$-1.9^{-0.8}_{-0.6}$	4^{+1}_{-2}	30^{+2}_{-12}
8	5	2	0.25	4	$2.1^{+1.0}_{-0.7}$	$10.3^{+1.0}_{-1.5}$	$32.7^{+3.8}_{-3.8}$	$14.2^{+1.7}_{-1.7}$	$33.3^{+6.4}_{-4.4}$	$14.5^{+2.7}_{-1.9}$	$-7.0^{+1}_{-0.8}$	$-1.8^{+1}_{-0.6}$	6^{+1}_{-3}	22^{+3}_{-2}
	…	…	0.5	4	$1.8^{+0.8}_{-0.7}$	$9.9^{+1.1}_{-1.9}$	$25.6^{+4.3}_{-6.9}$	$11.1^{+1.8}_{-3.0}$	$27.8^{+8.2}_{-5.8}$	$11.4^{+4.2}_{-2.0}$	$-6.5^{+0.8}_{-0.9}$	$-1.1^{+0.7}_{-0.8}$	3^{+2}_{-1}	24^{+1}_{-6}
	…	…	0.75	4	$1.6^{+0.8}_{-0.7}$	$9.6^{+1.2}_{-2.2}$	$20.5^{+6.5}_{-3.5}$	$8.9^{+2.6}_{-1.6}$	$28.5^{+7.0}_{-7.5}$	$10.9^{+4.4}_{-2.1}$	$-6.5^{+0.8}_{-0.9}$	$-1.1^{+0.7}_{-0.8}$	5^{+1}_{-3}	16^{+5}_{-1}
	…	…	1	4	$1.6^{+0.7}_{-0.8}$	$9.4^{+1.1}_{-2.5}$	$15.4^{+1.9}_{-1.7}$	$6.7^{+0.8}_{-0.8}$	$15.5^{+6.3}_{-2.2}$	$6.7^{+2.5}_{-0.8}$	$-7.0^{+1}_{-0.4}$	$-1.8^{+1}_{-0.2}$	8^{+2}_{-4}	40^{+1}_{-5}
8	5	1	0.05	4	$3.4^{+1.1}_{-1.1}$	$11.6^{+0.5}_{-1.0}$	$32.9^{+4.8}_{-4.8}$	$14.1^{+2.2}_{-2.2}$	$33.9^{+6.1}_{-5.1}$	$14.5^{+2.9}_{-2.1}$	$-6.4^{+0.6}_{-1}$	$-1.0^{+0.5}_{-1}$	3^{+3}_{-1}	22^{+7}_{-1}
20	12	2	0.05	2	$3.4^{+1.1}_{-1.1}$	$11.6^{+0.5}_{-1.0}$	$41.8^{+7.2}_{-4.6}$	$17.9^{+3.4}_{-1.8}$	$48.3^{+4.2}_{-8.6}$	$21.0^{+1.8}_{-4.0}$	$-6.2^{+0.7}_{-1}$	$-0.6^{+0.5}_{-1}$	16^{+2}_{-6}	60^{+9}_{-1}
2	1	2	0.05	18	$3.4^{+1.1}_{-1.1}$	$11.6^{+0.5}_{-1.0}$	37^{+30}_{-11}	$16^{+13}_{-4.8}$	39^{+26}_{-10}	17^{+11}_{-5}	$-6.7^{+0.8}_{-1}$	$-1.4^{+0.8}_{-1}$	0^{+4}_{-0}	3^{+1}_{-1}

Note. M_i is the initial cluster mass. # denotes the number of models simulated with the same initial cluster properties. Cluster formation redshifts, $z_{\rm form}$, and the equivalent look-back times, $t_{\rm lb}$, are shown for clusters of particular metallicities (Section 3.1). We denote the eccentricities of BBH orbits (that merge in $z \leqslant 1$) when their GW frequency $f_{\rm GW} = 10$ and 10^{-4} Hz by e_1 and e_{-4}, respectively. $N_{\rm merge}$ denotes the number of BBH mergers. All numbers with error bars denote the mode and 1σ range for the respective distributions.

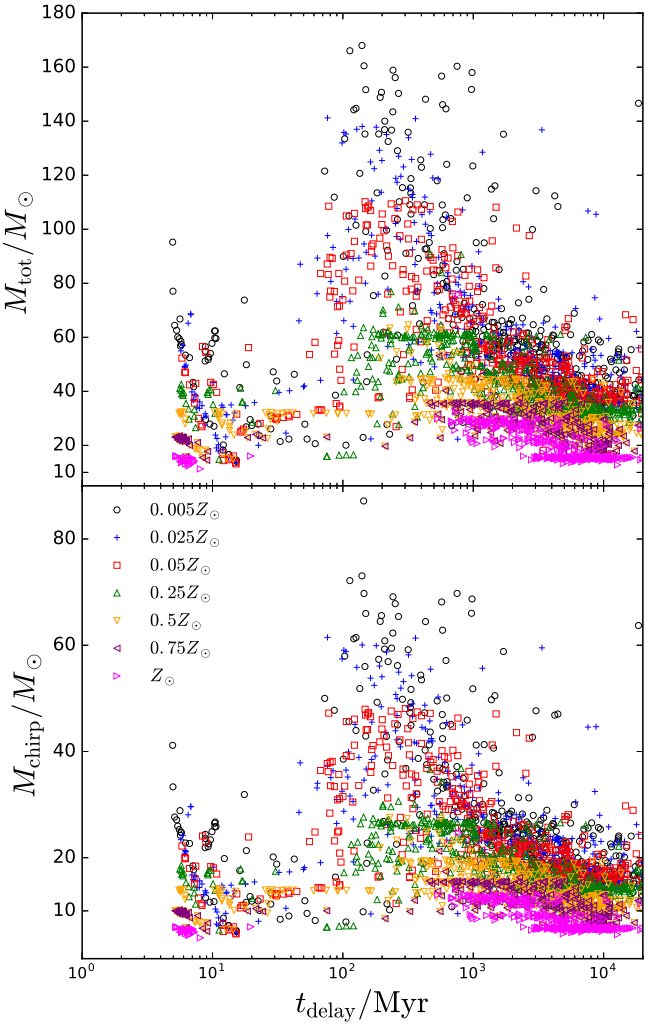

Figure 1. $t_{\rm delay}$ vs. $M_{\rm tot}$ (top) and $M_{\rm chirp}$ (bottom) for BBH mergers from clusters modeled with different metallicities. Black (circle), blue (plus), red (square), green (triangle-up), orange (triangle-down), purple (triangle-left), and magenta (triangle-right) denote clusters modeled with $Z/Z_\odot = 0.005$, 0.025, 0.05, 0.25, 0.5, 0.75, and 1, respectively. Merging BBHs from lower-metallicity clusters are more massive, a consequence of the Z-dependence of the BH mass function at formation (e.g., Belczynski et al. 2010). Heavier merging BBHs have shorter $t_{\rm delay}$ for any metallicity, a consequence of how BHs are dynamically processed inside clusters and the mass dependence of the inspiral time via GW radiation from a given initial separation (Peters 1964). Early ($t_{\rm delay} \lesssim 100$ Myr) mergers come from systems where both BH progenitors were in a primordial binary. The apparent overdensity of mergers at specific BBH masses for a given metallicity is due to spikes in the BH mass function at formation, expected from the state-of-the-art progenitor-to-remnant mass relation (Belczynski et al. 2010).

selected redshift values using a Gaussian kernel density estimator (KDE) with bandwidth determined by Scott's method (Scott 1992). We find that $f(z)_{\rm Z}$ can be distributed across a large range in redshift, especially for clusters with low metallicities. Furthermore, due to the sharp peak of SFR(z) at $z \simeq 2$, the modes of $f(z)_{\rm Z}$, even for the highest metallicities we consider, are pushed toward $z = 2$ (Figure 2; Table 1).

3.2. Properties of BBH Mergers within $0 \leqslant z \leqslant 1$

We take 500 random draws of $z_{\rm form}$ from $f(z)_{\rm Z'}$ (Equation (3); Figure 2) for clusters of a given metallicity, Z′. For each model of a particular metallicity and for each draw of $z_{\rm form}$ we map the window of interest for BBH merger

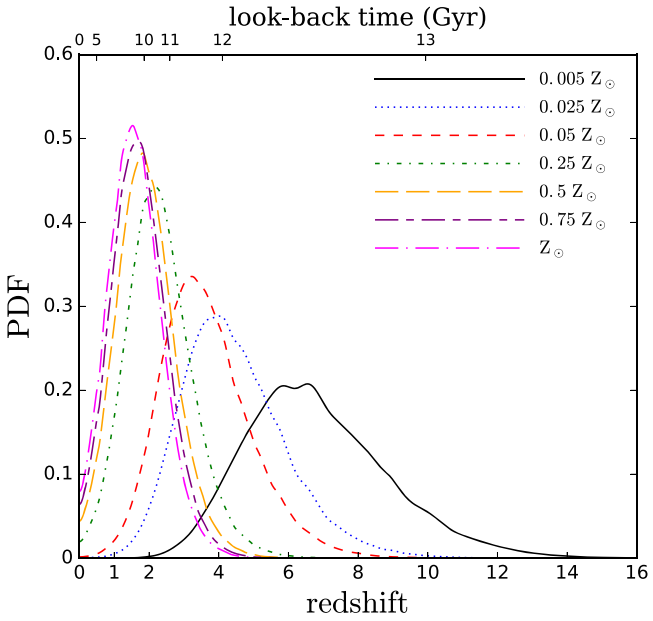

Figure 2. PDF for the redshift of formation ($z_{\rm form}$) for star clusters of different metallicities (Equation (3)). Black (solid), blue (dotted), red (dashed), green (dash–dot), orange (long-dash), purple (long-dash-short-dash), and magenta (long-dash–dot) lines denote clusters modeled with metallicities $Z/Z_\odot = 0.005$, 0.025, 0.05, 0.25, 0.5, 0.75, and 1, respectively. Look-back times corresponding to $z_{\rm form}$ are also shown for reference.

redshifts, Δz (e.g., $0 \leqslant z \leqslant 1$), to the corresponding window in $t_{\rm delay}$, and collect all BBH mergers within Δz. This essentially acts as a sliding window of selection of BBH mergers within Δz from a cluster based on the distribution of that cluster's formation times. We create a multi-dimensional (redshift, M_p, and M_s) PDF from the selected BBH mergers from all cluster models of a given set of initial properties. We then draw a sample of 10^5 BBH mergers from this PDF to investigate the BBH merger properties for each metallicity.

Figure 3 shows the distributions for $M_{\rm tot}$ and $M_{\rm chirp}$ for the merging BBHs from clusters with seven different metallicities. We find that the mass distributions are insensitive to the exact choice of σ for $f'(Z)_z$ (Section 3.1). The left panels show 1σ contours for BBH mergers in the mass–redshift plane. The right panels show the mass distributions for BBHs merging in $z \leqslant 0.2$. For any metallicity, the 1σ contours encompass higher masses as redshift increases. This is because the lower the $t_{\rm delay}$ (equivalent to higher redshift), the higher the mass of merging BBHs (Figure 1). The mass distributions, even from clusters of vastly different metallicities, show significant overlap for any $z \leqslant 1$ (Figure 3) primarily due to the wide ranges in merger masses for any $t_{\rm delay}$ and metallicity (Figure 1). This makes uniquely inferring the metallicity of a particular merging BBH hard. Lower-metallicity clusters form higher-mass BBHs because BHs formed from lower-metallicity progenitors are heavier. However, lower-metallicity clusters are older, hence, a particular observation window in redshift corresponds to higher $t_{\rm delay}$ and thus lower masses of merging BBHs (Figure 1). For the same reasons, the mass distributions and their peaks for local BBH mergers do not change significantly for any $Z/Z_\odot \lesssim 0.05$ (Figure 3; Table 1).

We compare the intrinsic mass distributions of BBH mergers from models with the source-frame $M_{\rm chirp}$ of the detected GW sources. $M_{\rm chirp}$ for LVT151012 and GW151226 are within 1σ of the $M_{\rm chirp}$ distributions for BBHs merging in $z \leqslant 0.2$ from

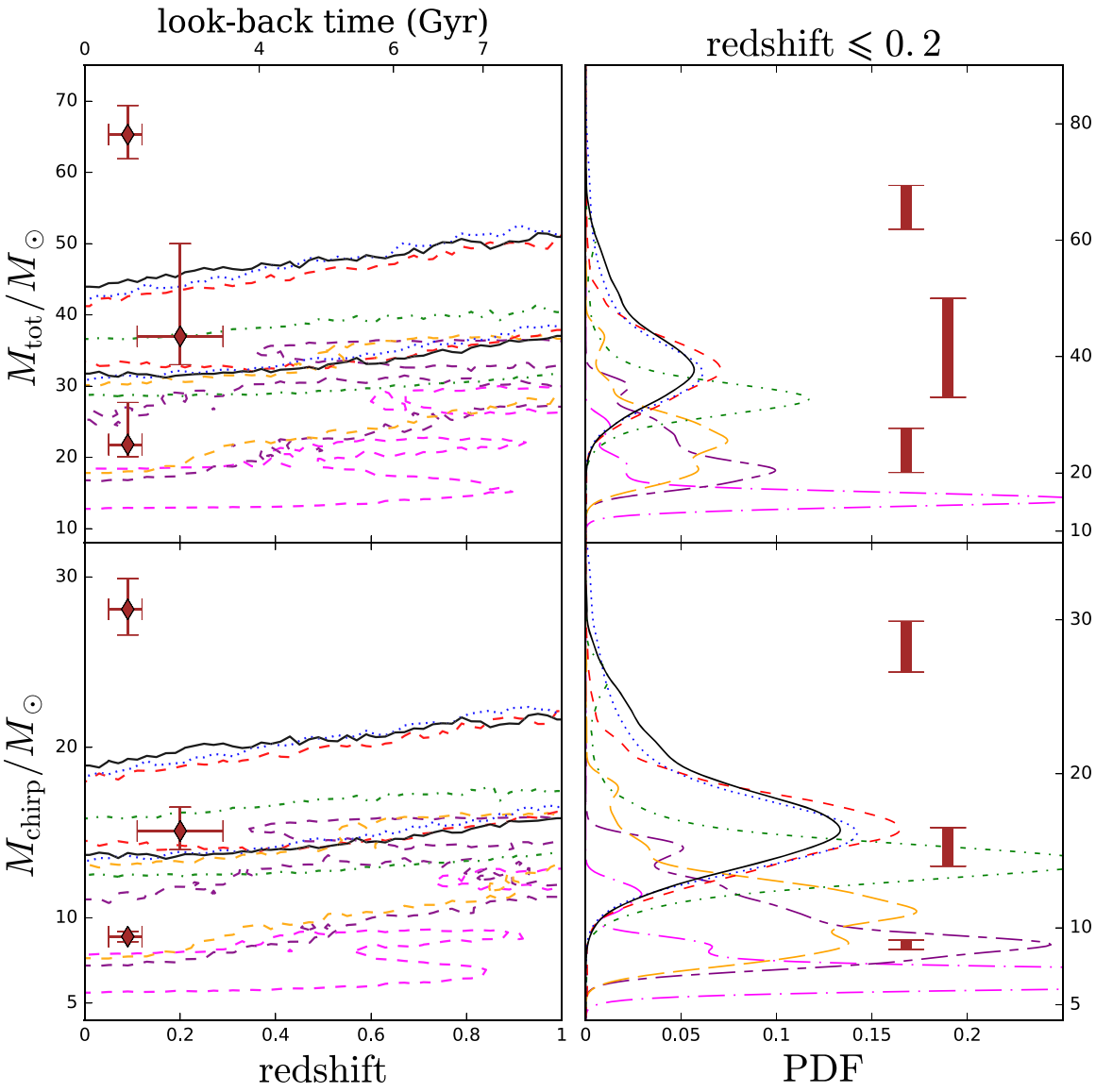

Figure 3. Right: mass distributions for BBHs merging in $z \leqslant 0.2$. Left: 1σ contours of the mass distributions of BBHs as a function of their merger redshift. Top and bottom panels show $M_{\rm tot}$ and $M_{\rm chirp}$. Line colors (and styles) have the same meaning as in Figure 2. Brown diamonds and error bars denote the source-frame properties and 90% confidence intervals for the detected BBH mergers (Abbott et al. 2016b).

models with $Z/Z_\odot \leqslant 0.25$ and $Z/Z_\odot \geqslant 0.5$, respectively. Moreover, $M_{\rm chirp}$ for LVT151012 and GW151226 line up perfectly with the peaks for $Z/Z_\odot = 0.25$ and 0.75, respectively (Figure 3; Table 1). $M_{\rm chirp}$ for GW150914 is within 2σ of the $M_{\rm chirp}$ distributions for $Z/Z_\odot \leqslant 0.05$, but is higher than 1σ of the $M_{\rm chirp}$ distributions for any metallicities we consider. Since for $Z/Z_\odot \lesssim 0.05$, $M_{\rm chirp}$ distributions are not sensitive to the cluster metallicity (Figure 3), GW150914 is likely more massive than intrinsically typical BBHs merging in $z \leqslant 0.2$. Accounting for detectability of BBH mergers by aLIGO, especially from low-metallicity clusters because the larger range of merger masses from them, would significantly reduce and enhance low- and high-mass regions of the PDF, respectively, making GW150914 less rare among *detectable* BBH mergers from old, low-metallicity clusters (Rodriguez et al. 2016b). Keeping this in mind, it is actually not surprising that the first ever detected GWs came from the merger of an intrinsically unusually massive BBH. BH dynamics in a star cluster increases BBH masses (via repeated exchange encounters; e.g., Rodriguez et al. 2015) and $t_{\rm delay}$ (S. Chatterjee et al. 2017, in preparation) relative to BBHs formed in isolation. Thus, for a given metallicity and $z_{\rm form}$, it is likely harder to create BBH mergers as massive as GW150914 in isolation in the local universe.

3.3. Variation Due to Initial Cluster Properties

We now investigate how sensitive our results are on the initial cluster properties. The escape speed of the cluster, set by the cluster mass, sets the separation of the binaries at ejection, and thus $t_{\rm delay}$. The relaxation timescale ($t_{\rm relax}$) controls the timescale for dynamical processing of BHs. Variations in initial N and r_v capture both of these effects. While the merger rates do depend on other variations, e.g., in the initial binary fraction and binary orbital properties of high-mass stars, the stellar IMF, and the distribution of natal kicks, the mass distribution of BBHs merging in the local universe is insensitive to these variations (Chatterjee et al. 2017).

We find that the masses of local mergers from clusters of the same metallicity ($Z/Z_{\odot} = 0.05$) do not change significantly due to variations in initial N and r_v. The modes of the distributions for both $M_{\rm tot}$ and $M_{\rm chirp}$ are well within 1σ of each other even when the initial N is changed by an order of magnitude, and the initial r_v is changed by a factor of 2 (Table 1). Nevertheless, clusters with lower initial r_v processes through the BHs quicker due to their shorter $t_{\rm relax}$. Hence, the distribution is pushed toward slightly lower masses as r_v is decreased (Table 1). On one hand, a higher-N cluster (keeping all else fixed) ejects BBHs that are tighter, reducing $t_{\rm delay}$ (e.g., Rodriguez et al. 2016a). On the other hand, higher-N increases $t_{\rm relax}$, resulting in slower dynamical processing of BHs and slower decrease of $M_{\rm chirp}$ with respect to $t_{\rm delay}$ (Figure 1; e.g., Morscher et al. 2015). These competing effects make the mass distributions for BBHs merging in $z \lesssim 0.2$ insensitive to the initial N of the parent cluster. However, we caution that this trend should not be extrapolated to very low-N clusters that dissolve before significant dynamical processing of their BHs, or to very high-N clusters where $t_{\rm relax}$ is longer than the cluster age.

We have also followed the eccentricities of BBH orbits merging in $z \leqslant 1$ using the quadrupole approximated GW orbital evolution equations (Peters 1964). We find the e-distributions as the BBHs enter the aLIGO (10 Hz) and LISA (10^{-4} Hz) frequency bands ($f_{\rm GW}$; Wen 2003). Similar to Breivik et al. (2016), we find that at $f_{\rm GW} = 10$ Hz BBHs have very low $e \sim 10^{-7}$. Whereas, $e \sim 0.01$–0.4 for the BBH orbits when $f_{\rm GW} = 10^{-4}$ Hz.[4] We find no clear trends in the distributions of $\log e$ at these frequencies depending on metallicity, N, or r_v (Table 1).

4. Conclusion

We have studied the effects of the parent cluster's metallicity (and metallicity-dependent age) on the BBH masses merging in the local universe. Assuming cluster origin, we have found likely cluster properties of detected GW sources by comparing detected masses with mass distributions from models (Section 3.2; Figure 3). We find that $M_{\rm chirp}$ of GW150914 is not within 1σ of the intrinsic $M_{\rm chirp}$ distributions for BBHs merging in $z \leqslant 0.2$ for any metallicities we consider, but is within 2σ for mergers from clusters with $Z/Z_{\odot} \leqslant 0.05$. Since below $Z/Z_{\odot} = 0.05$ the $M_{\rm chirp}$-distribution is insensitive to metallicity and dynamically created BBHs are generally heavier than those produced in isolation for any given metallicity, mergers of BBHs as massive as GW150914 in $z \leqslant 0.2$ are likely intrinsically rare. Of course, detection biases push the observed distributions toward higher masses. Since the lower the metallicity, the larger the range in merging BBH masses, detection biases would affect the mass distributions from lower-metallicity clusters more. Thus, the *detection* of mergers like GW150914 would be less rare (Rodriguez et al. 2016b). $M_{\rm chirp}$ of LVT151012 is near the peak of the distribution from clusters modeled with $Z/Z_{\odot} = 0.25$, and is within 1σ of the distributions from all clusters modeled with $Z/Z_{\odot} \leqslant 0.25$. $M_{\rm chirp}$ of GW151226 is closest to the peak of $M_{\rm chirp}$-distribution from clusters with $Z/Z_{\odot} = 0.75$ and is within 1σ from clusters with $Z/Z_{\odot} \geqslant 0.5$ Thus, assuming cluster origin, GW151226 likely formed in a higher-metallicity, younger cluster than typical GGCs.

We find several additional notable trends. Less massive BBHs have longer $t_{\rm delay}$ for any metallicities (Figure 1) since clusters dynamically form, process, and eject heavier BBHs earlier due to mass segregation (e.g., Morscher et al. 2015). Lower-metallicity clusters typically have higher $z_{\rm form}$ (Figure 2). Hence, BBHs from lower-metallicity clusters require longer $t_{\rm delay}$ to merge in $z \lesssim 0.2$. Lower metallicity leads to the formation of heavier BBHs (e.g., Fryer et al. 2012), but longer $t_{\rm delay}$ decreases merging BBH masses (Figure 1). Hence, while the expected trend is an increase of BBH masses merging in $z \lesssim 0.2$ as metallicity decreases, the mass distributions for local BBH mergers become insensitive to metallicity for $Z/Z_{\odot} \lesssim 0.05$.

Furthermore, we find that the masses of local BBH mergers are not very sensitive to the initial N or r_v even when N is varied over an order of magnitude and r_v by a factor of 2 (Table 1). This indicates that the metallicity and metallicity-dependent age of the parent cluster are likely the most important properties to determine the peaks and distributions of BBH masses merging in the local universe.

This work was supported by NSF grant AST-1312945, NSF grant PHY-1307020, and NASA grant NNX14AP92G. C.R. is grateful for the hospitality of the Kavli Institute for Theoretical Physics, supported by NSF grant PHY11-25915, and is supported at MIT by a Pappalardo Fellowship in Physics. V.K. and F.A.R. also acknowledge support from NSF grant PHY-1066293 at the Aspen Center for Physics.

[4] We neglect hierarchical triples that contribute at ~1% level for clusters (Antonini et al. 2016).

References

Abbott, B. P., Abbott, R., Abbott, T. D., et al. 2016a, ApJL, 818, L22
Abbott, B. P., Abbott, R., Abbott, T. D., et al. 2016b, PhRvX, 6, 041015
Abbott, B. P., Abbott, R., Abbott, T. D., et al. 2016c, PhRvL, 116, 241103
Abbott, B. P., Abbott, R., Abbott, T. D., et al. 2016d, PhRvL, 116, 061102
Antonini, F., Chatterjee, S., Rodriguez, C. L., et al. 2016, ApJ, 816, 65
Askar, A., Szkudlarek, M., Gondek-Rosińska, D., Giersz, M., & Bulik, T. 2017, MNRAS, 464L, 36
Banerjee, S., Baumgardt, H., & Kroupa, P. 2010, MNRAS, 402, 371
Barmby, P., Kuntz, K. D., Huchra, J. P., & Brodie, J. P. 2006, AJ, 132, 883
Bastian, N., Gieles, M., Lamers, H. J. G. L. M., Scheepmaker, R. A., & de Grijs, R. 2005, A&A, 431, 905
Belczynski, K., Buonanno, A., Cantiello, M., et al. 2014, ApJ, 789, 120
Belczynski, K., Dominik, M., Bulik, T., et al. 2010, ApJL, 715, L138
Belczynski, K., Holz, D. E., Bulik, T., & O'Shaughnessy, R. 2016a, Natur, 534, 512
Belczynski, K., Kalogera, V., & Bulik, T. 2002, ApJ, 572, 407
Belczynski, K., Repetto, S., Holz, D. E., et al. 2016b, ApJ, 819, 108
Breen, P. G., & Heggie, D. C. 2013, MNRAS, 432, 2779
Breivik, K., Rodriguez, C. L., Larson, S. L., Kalogera, V., & Rasio, F. A. 2016, ApJL, 830, 18
Chatterjee, S., Fregeau, J. M., Umbreit, S., & Rasio, F. A. 2010, ApJ, 719, 915
Chatterjee, S., Rodriguez, C. L., & Rasio, F. A. 2017, ApJ, 834, 68
Chatterjee, S., & Tan, J. C. 2012, ApJ, 754, 152
Chatterjee, S., Umbreit, S., Fregeau, J. M., & Rasio, F. A. 2013, MNRAS, 429, 2881
de Mink, S. E., & Mandel, I. 2016, MNRAS, 460, 3545
Dominik, M., Belczynski, K., Fryer, C., et al. 2012, ApJ, 759, 52
Dominik, M., Belczynski, K., Fryer, C., et al. 2013, ApJ, 779, 72
Dominik, M., Berti, E., O'Shaughnessy, R., et al. 2015, ApJ, 806, 263
Dvorkin, I., Vangioni, E., Silk, J., Uzan, J.-P., & Olive, K. A. 2016, MNRAS, 461, 3877
Fregeau, J. M., Gürkan, M. A., Joshi, K. J., & Rasio, F. A. 2003, ApJ, 593, 772
Fregeau, J. M., & Rasio, F. A. 2007, ApJ, 658, 1047
Fryer, C. L., Belczynski, K., Wiktorowicz, G., et al. 2012, ApJ, 749, 91
Harris, W. E. 1996, AJ, 112, 1487
Heggie, D., & Hut, P. 2003, The Gravitational Million-Body Problem: A Multidisciplinary Approach to Star Cluster Dynamics (Cambridge: Cambridge Univ. Press)

Hurley, J. R., Pols, O. R., & Tout, C. A. 2000, MNRAS, 315, 543
Hurley, J. R., Tout, C. A., & Pols, O. R. 2002, MNRAS, 329, 897
Kowalska-Leszczynska, I., Regimbau, T., Bulik, T., Dominik, M., & Belczynski, K. 2015, A&A, 574, A58
Kroupa, P. 2001, MNRAS, 322, 231
Madau, P., & Dickinson, M. 2014, ARA&A, 52, 415
Mandel, I., & de Mink, S. E. 2016, MNRAS, 458, 2634
Marchant, P., Langer, N., Podsiadlowski, P., Tauris, T. M., & Moriya, T. J. 2016, A&A, 588, A50
Morscher, M., Pattabiraman, B., Rodriguez, C., Rasio, F. A., & Umbreit, S. 2015, ApJ, 800, 9
Pattabiraman, B., Umbreit, S., Liao, W.-K., et al. 2013, ApJS, 204, 15
Peters, P. C. 1964, PhRv, 136, 1224
Rodriguez, C. L., Chatterjee, S., & Rasio, F. A. 2016a, PhRvD, 93, 084029
Rodriguez, C. L., Haster, C.-J., Chatterjee, S., Kalogera, V., & Rasio, F. A. 2016b, ApJL, 824, L8
Rodriguez, C. L., Morscher, M., Pattabiraman, B., et al. 2015, PhRvL, 115, 051101
Rodriguez, C. L., Morscher, M., Wang, L., Chatterjee, S., et al. 2016c, MNRAS, 463, 2109
Scheepmaker, R. A., Haas, M. R., Gieles, M., et al. 2007, A&A, 469, 925
Scott, D. W. 1992, Multivariate Density Estimation (New York: Wiley)
Vink, J. S., de Koter, A., & Lamers, H. J. G. L. M. 2001, A&A, 369, 574
Wen, L. 2003, ApJ, 598, 419
Ziosi, B. M., Mapelli, M., Branchesi, M., & Tormen, G. 2014, MNRAS, 441, 3703